International Journal of Applied Earth Observation and Geoinformation 130 (2024) 103879

Contents lists available at ScienceDirect

International Journal of Applied Earth Observation and Geoinformation

journal homepage: www.elsevier.com/locate/jag

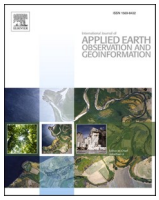

Assessment of soil salinity using explainable machine learning methods and Landsat 8 images

Samet Aksoy [a], Elif Sertel [a,*], Ribana Roscher [b], Aysegul Tanik [c], Nikou Hamzehpour [d]

[a] Department of Geomatics Engineering, Faculty of Civil Engineering, Istanbul Technical University (ITU), 34469 Maslak, Istanbul, Turkey
[b] Institute of Bio- and Geosciences, Plant Sciences, Forschungszentrum Jülich GmbH, 52428 Jülich, Germany
[c] Department of Environmental Engineering, Faculty of Civil Engineering, Istanbul Technical University (ITU), 34469 Maslak, Istanbul, Turkey
[d] Department of Soil Science and Engineering, Faculty of Agriculture, University of Maragheh, Maragheh, Iran

ARTICLE INFO

Keywords:
Soil salinity
Google Earth Engine
SHAP
XAI
Landsat-8 OLI
Machine learning

ABSTRACT

The aim of this study is to comparatively analyze the performance of machine learning (ML) algorithms for modeling soil salinity using field-based electrical conductivity (EC) data and Landsat-8 OLI satellite images with derived environmental covariates. We also aim to interpret and explain the ML models with and without over-sampling methods using Shapley (SHAP) values, an explainable ML approach that has not yet been utilized for soil salinity estimation tasks as an ML problem. We investigate two case study areas from western and south-eastern Lake Urmia Playas (LUP) in the Northwest of Iran. Our study uses 26 environmental covariates, two ML models, namely extreme gradient boosting (XGBoost) and random forest (RF), and two over-sampling methods: synthetic minority over-sampling technique (SMOTE) and random over-sampling (ROS). Results indicate that XGBoost performs better compared to RF in terms of both R2 and RMSE. Additionally, the visual interpretation of soil salinity maps demonstrated the superiority of XGBoost. SMOTE produced superior results than ROS and no over-sampling test cases. Finally, SHAP analysis illustrated that vegetation indices made a greater contribution to the soil salinity prediction in the West LUP, while visible bands contributed more in the Southeast LUP Region.

1. Introduction

Soil is the environment for habitats, with wide biodiversity extending from micro to macro scales. Water is an essential natural resource directly affecting life on and in the soil (Brevik et al., 2015). Healthy soil is vital for plant growth, meeting the nutritional needs of people, and water filtration. In addition, it supports land to be more resilient against disasters such as floods, droughts, and fires and plays a role in regulating climatic conditions. Soil degradation or substantial alterations can arise from both natural and human-induced factors, underscoring the significance of proactive measures to preserve soils and biodiversity. Human-induced modifications to soil structure often stem from inadequate management of cultivation and irrigation practices, with soil salinization being a notable consequence (Masoud et al., 2019; Stavi et al., 2021).

Soil salinity can be caused either by anthropogenic or natural factors. Although it might increase over time due to natural causes, man-made aspects such as agricultural activities accelerate its occurrence. It affects especially semi-arid and arid regions of the world. Drought events, which climate change has made more frequent, have brought this problem to a global scale in the recent years (Stavi et al., 2021; Ge et al., 2022).

According to the Food and Agriculture Organization of the United Nations (FAO), 3 % of the world's soils are affected by salinity in the upper and 6 % in the lower layers (FAO, 2023). Salinization of soils in agricultural areas causes excessive economic losses. As the severity of soil salinity increases, the yield of plants decreases, and plants lose their vitality after a certain level. Thus, it is a dynamic problem that depends on soil structure, hydrological and climatic conditions, and agricultural, social, and economic balances (Allbed and Kumar, 2013; Aksoy et al., 2022). Monitoring and detecting soil salinity by applying only laboratory analyses and field surveys are not efficient enough for large-scale salt-affected lands. Nowadays, remote sensing (RS) techniques, machine learning (ML) approaches, and geographic information systems (GIS) are regarded as modern tools to analyse and model this phenomenon (Wang et al., 2019; Chen et al., 2021; Aksoy et al., 2022). RS and field-measured electrical conductivity (EC) data are integrated and used commonly to model and accurately map soil salinity (Gorji et al., 2020;

* Corresponding author.
E-mail address: sertele@itu.edu.tr (E. Sertel).

https://doi.org/10.1016/j.jag.2024.103879
Received 19 September 2023; Received in revised form 10 February 2024; Accepted 27 April 2024
Available online 3 May 2024
1569-8432/© 2024 The Authors. Published by Elsevier B.V. This is an open access article under the CC BY-NC license (http://creativecommons.org/licenses/by-nc/4.0/).

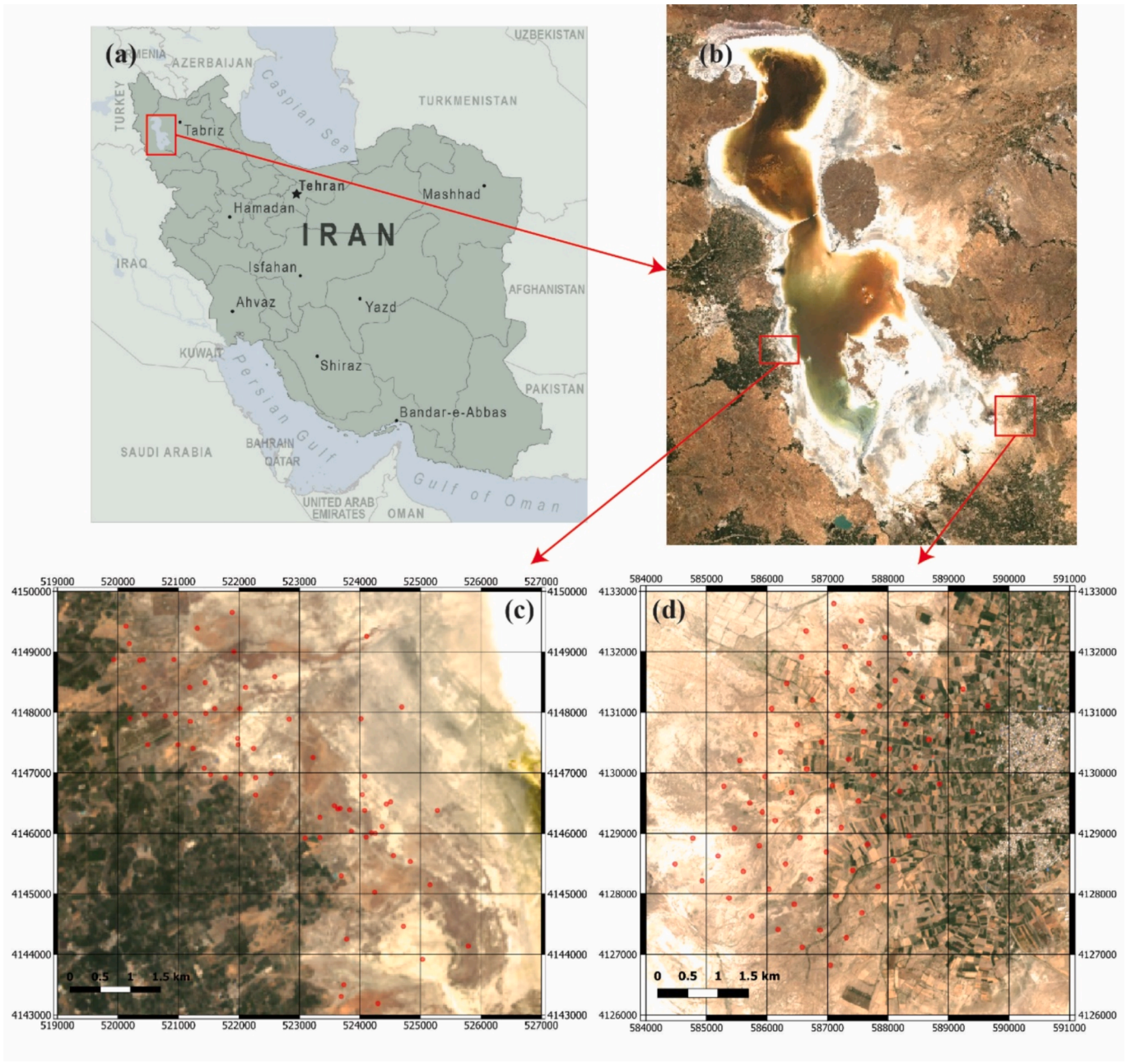

Fig. 1. Study areas: (a) location of Lake Urmia in Iran, (b) view of the lake and case study areas, (c) West LUP, (d) Southeast LUP.

Stavi et al., 2021). RS systems can differentiate saline soils from non-saline soils as their spectral responses differ. However, slightly or moderately saline soil cannot be identified easily because other soil minerals and their components change the spectral behavior of the soil surface (Allbed and Kumar, 2013). Soil salinity severities are classified into five classes, from non-saline to extremely saline, based on deci Siemens per meter (dS/m) at 25 °C and represented by EC values.

Recent advancements in machine learning and artificial intelligence have significantly contributed to the development of more resilient digital soil mapping techniques, offering dependable predictive methods for evaluating salinization (Sahbeni et al., 2023; Aksoy et al., 2022; Gu et al., 2022; Mohammadifar et al., 2022; Zarei et al., 2021; Wang et al., 2019). Random Forest (Kabiraj et al., 2022), Support Vector Regression (Taghizadeh et al., 2021), and XGBoost (Zarei et al., 2021) are the most widely used machine learning methods for soil salinity mapping using remotely sensed data and field measurements. Some of deep learning models used for soil salinity mapping are deep convolutional neural networks (DCNNs) (Garajeh et al., 2021), densely connected deep neural networks (DenseDNNs), recurrent neural networks (RNNs) RNN with long short-term memory (RNN-LSTM) (Mohammadifar et al., 2021), U-Net (Akca and Gungor, 2022), U^2-Net (Gu et al., 2022), and Deep Boltzmann machine (DBM) (Mohammadifar et al., 2022). Mohammadifar et al. (2021) compared DL models performance to ML model, and find out that DL models outperformed shallow learning models for soil salinity modeling. The study utilized a dataset consisting of 319 soil samples with electrical conductivity (EC) values ranging from 1.2 to 13.11 deciSiemens per meter (ds/m), with a mean EC value of 6.1 ds/m. Importantly, the dataset did not include soil samples from the highly saline class. In their investigation, Akca and Gungor (2022) employed the U-Net and Support Vector Machine (SVM) algorithms for predicting soil salinity in the Harran Plain. The study utilized electrical conductivity (EC) values measured at 509 points and Rapideye satellite

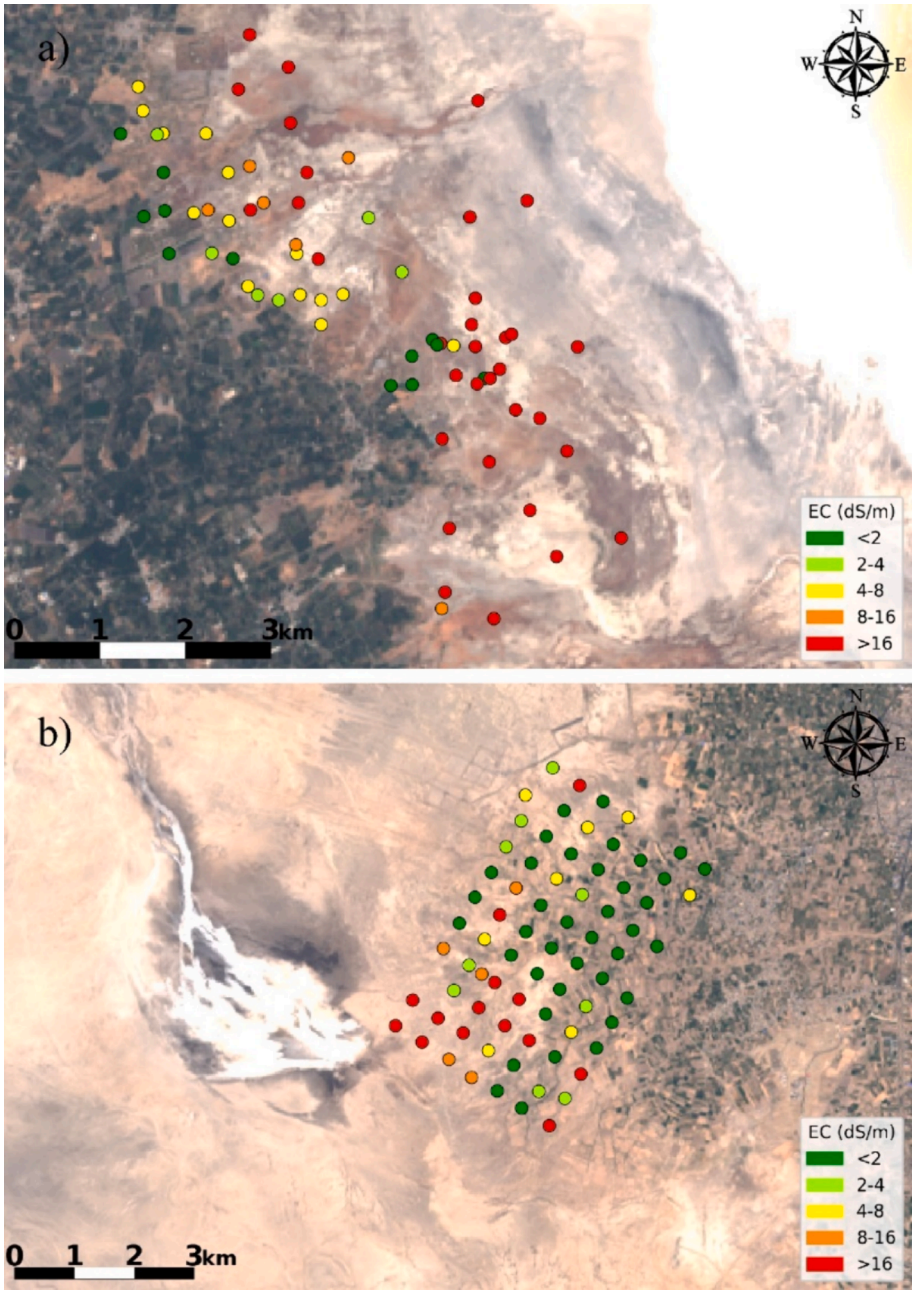

Fig. 2. Spatial distribution of soil samples (a) West LUP, (b) Southeast LUP.

imagery. Their analysis revealed the superior performance of the U-Net algorithm in soil salinity prediction compared to SVM. It is noteworthy that the XGBoost algorithm was not included in the ML models used in these studies. The utilization of DL-based methods is hindered by their data-hungry training process (Marcus, 2018). Consequently, this study exclusively employs ML-based methods due to the limited nature of the ground-truth data (less than 100 for each site). Refining ML-based methods using XAI is a new approach in the literature. This study aims to use RS data and in-situ soil measurements to determine the spatial distribution of soil salinity with different ML-based regression methods. The objectives are to:

- Investigate the capacity of Landsat-8 OLI satellite imagery in determining soil salinity for two highly saline study areas in Iran;
- Evaluate the efficiency and utility of RF and XGBoost ML models for modeling soil salinity;
- Examine the effect of different features on the prediction accuracy of ML models;
- Understand and explain the results of implemented ML models using explainable artificial intelligence methods in detail.

To fulfill our objectives, we collected 26 features comprising different spectral bands of a Landsat-8 OLI image and different indices created from these bands. We trained two widely-used ML-based regression models using these features and in-situ salinity measurements. In this study, the selection of the Random Forest (RF) algorithm was based on its well-documented success in soil salinity modeling, as evidenced by Sahbeni et al. (2023). Furthermore, the decision to include the XGBoost algorithm for comparison was influenced by its increasing popularity and its regularization capability to prevent overfitting through regularization (Ma et al., 2023; Zarei et al., 2021. We also employed different data over-sampling methods to minimize the

Table 1
EC ranges and sample counts in each salinity class.

Study area	Total collected samples	Number of modeling samples	Number of validation samples	EC ranges	0–2 dS/m	2–4 dS/m	4–8 dS/m	8–16 dS/m	Above 16dS/m
West LUP	71	39	10	0–102	12	6	14	6	33
Southeast LUP	74	49	19	0–107	38	9	8	5	14

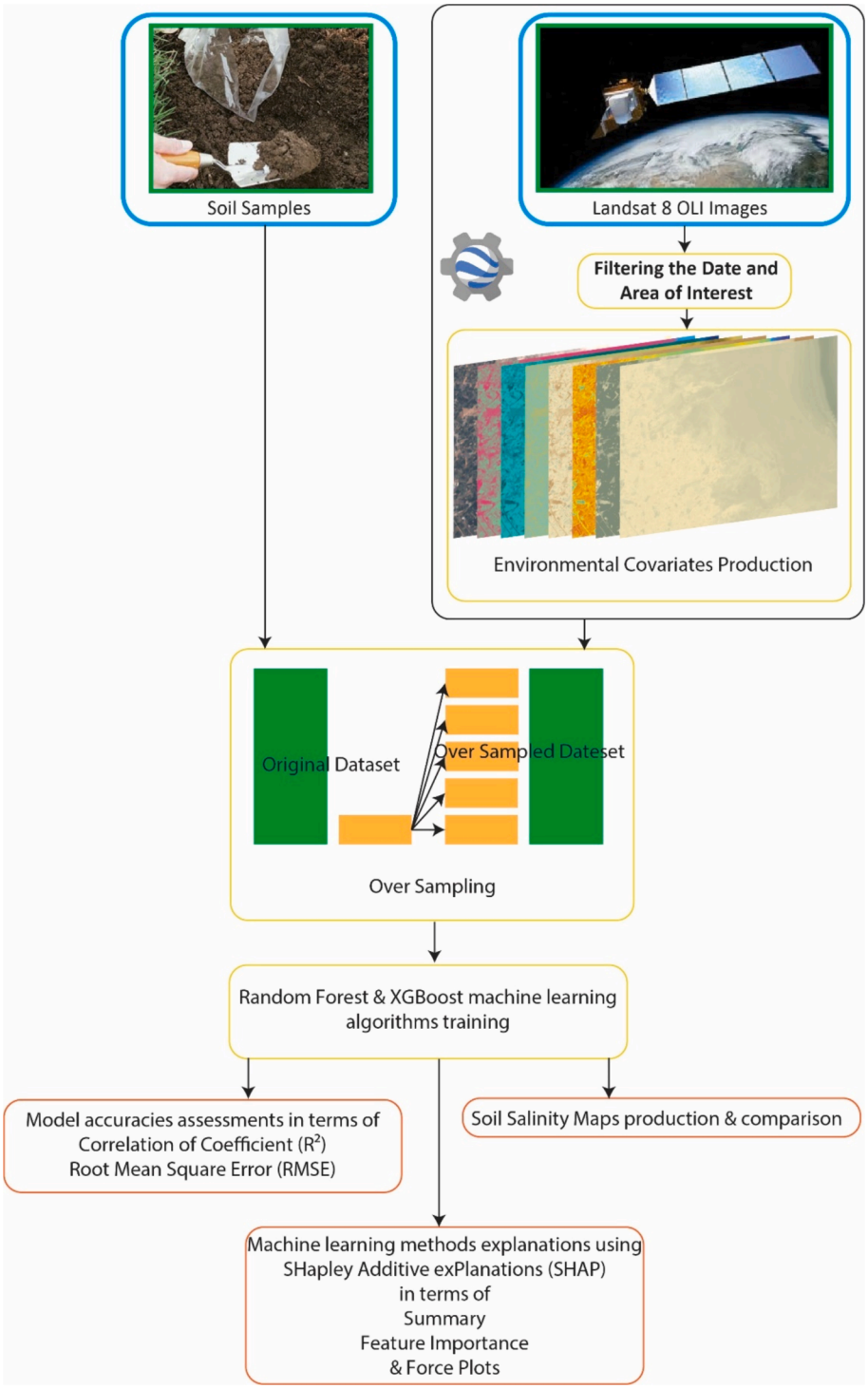

Fig. 3. Flow diagram of the methodology used.

Data	Features	Code	Formula
Landsat 8 OLI	Blue, Green, Red, NIR, SWIR1, SWIR2		
	Tasseled Cap	TC1,2,3	
Vegetation Indices	Normalized Difference Vegetation Index	NDVI	(NIR – Red) / (NIR + Red)
	Extended NDVI	ENDVI	(NIR + SWIR2 – Red) / (NIR + SWIR2 + Red)
	Enhanced Vegetation Index	EVI	[2.5 * (NIR – Red)] / [NIR + 6*Red – 7.5*Blue]
	Two-band enhanced vegetation index	EVI2	[2.5 * (NIR – Red)] / (NIR + 2.4*Red -1)
	Canopy Response Salinity Index	CRSI	$([(NIR*Red) – (Green*Blue)] / [(NIR*Red) + (Green*Blue)])^{0.5}$
	Extended EVI	EEVI	2.5*(NIR + SWIR1 – Red) / [NIR+2.5*(SWIR1+6*NIR+7.5*SWIR1)*Blue + 1]
	Generalized Difference Vegetation Index	GDVI	$(NIR^2 - Red^2) / (NIR^2 + Red^2)$
	Soil Adjusted Vegetation Index	SAVI	[(NIR – Red) * (1 + L)] / (NIR + Red + L); L = 0.5
	Simple Ratio vegetation index	SR	NIR / Red
Water Index	Normalized Difference Water Index	NDWI	(Green – NIR) / (Green + NIR)
Salinity Indices	Salinity Index 1	SI1	(Blue*Red)/Green
	Salinity Index 2	SI2	$(Blue * Red)^{0.5}$
	Salinity Index 3	SI3	(Green + Red)/2
	Salinity Index 4	SI4	(Green * Red)0.5
	Salinity Index 5	SI5	Blue / Red
	Salinity Index 6	SI6	(Red * NIR) / Green
	Salinity Index 7	SI7	2* Green – 5*(Red + NIR)

Fig. 4. Environmental covariates used in this study.

problems arising from the limited number of reference data. Finally, we explained the trained ML models in terms of the contributions of the features by applying explainable ML methods. This paper seeks to close a gap in the literature on RS-based soil salinity through investigating the over-sampling methods with the intention of increasing the limited ground measurements and integrating XML to better explain the ML-based models used in soil salinity mapping. In addition, a comprehensive analysis of two different case study regions provides insights into other locations suffering from soil salinity.

2. Study regions and datasets

2.1. Study regions

We examined two areas around Lake Urmia in Iran, West Urmia Playa and Bonab Region, shown in Fig. 1(a) and (b). Lake Urmia is a large saline lake with an area of 6000 km^2. This lake has been declared as a natural park since 1976 and is on the UNESCO protection list. It has a basin of 51876 km^2 and 6.5 million people benefit from this basin through agricultural and industrial activities. Although agricultural areas cover 10 % of the area, they consume 90 % of the renewable water resources for irrigation (Haghighi et al., 2018). Due to reasons such as excessive water consumption and insufficient rainfall, the water surface area has shrunk over time. An increase in water consumption caused excessive use of groundwater, and consequently, salty groundwater reduced agricultural productivity over time. Agricultural lands with reduced productivity started to be abandoned (Hamzehpour et al., 2018; Aksoy et al., 2022).

2.1.1. Western Lake Urmia Playa

The first case study area is in the western part of Lake Urmia Playa (LUP) (Fig. 1(b) and (c)). It is approximately 82 km^2 with an elevation varying between 1270 and 1278 m. 71 soil samples are collected from different playa surfaces identified previously (Hamzehpour et al., 2022) and EC is determined in the laboratory in 1:2.5 soil-to-water extracts using a Jenwey conductivity meter (model 45 10). The samples are collected from the top 20 cm of the soil during October 2–12, 2018 (Fig. 2) representing the end of the dry season when salt accumulation is the highest.

2.1.2. Southeast Lake Urmia Playa

The second case study area is in the southeastern part of the LUP in the Bonab region (Fig. 1(a), (b), and (d)). The altitude of the region varies between 1270 m and 1285 m. 74 soil samples are collected from different playa surfaces identified previously in the region (Motaghi et al., 2020) from 0 to 20 cm depth during Autumn 2014, and soil EC is determined using the method explained in Section 2.1.1.

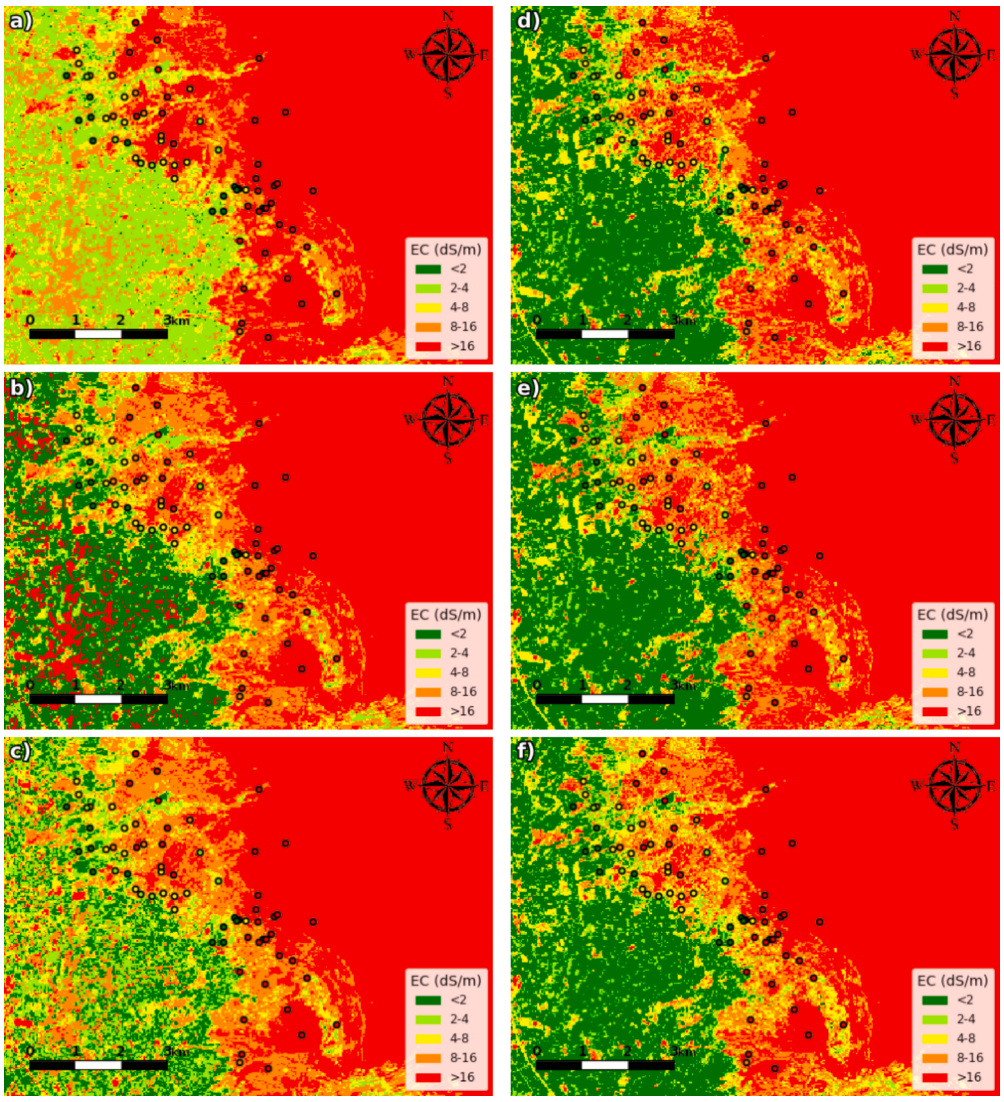

Fig. 5. Western LUP salinity maps (a) RFR and no over-sampling, (b) RFR and ROS, (c) RFR and SMOTE, (d) XGBoost and no over-sampling, (e) XGBoost and ROS, (f) XGBoost and SMOTE.

Table 2
Accuracy results of ML models for the West LUP.

ML Method	Over-sampling Method	R^2	RMSE
RFR	None	0.61	20.17
RFR	ROS	0.68	18.90
RFR	SMOTE	0.61	20.33
XGR	None	0.67	18.64
XGR	ROS	**0.76**	**16.60**
XGR	SMOTE	0.71	17.93

2.2. Satellite images

Landsat-8 OLI satellite image dated September 15, 2014 is used for the Southeast LUP, while the satellite image dated October 3, 2018 is chosen for the West LUP. Landsat-8 satellite completes its orbit at an altitude of 705 km in 99 min. Its temporal resolution is 16 days. We used Landsat-8 collection 2 level 1 imagery and geometrically and radiometrically corrected these images. Satellite-level reflectance values were used (USGS, 2022).

Table 3
Examination of salinity levels of the West LUP test samples.

Sample	GT	RFR None	RFR ROS	RFR SMOTE	XGR None	XGR ROS	XGR SMOTE
1	0–2	4–8	4–8	2–4	4–8	4–8	2–4
2	0–2	2–4	0–2	2–4	0–2	0–2	0–2
3	2–4	8–16	8–16	8–16	4–8	8–16	4–8
4	2–4	2–4	2–4	2–4	2–4	2–4	0–2
5	4–8	8–16	8–16	8–16	4–8	8–16	8–16
6	4–8	4–8	4–8	4–8	2–4	0–2	2–4
7	8–16	8–16	8–16	8–16	8–16	8–16	4–8
8	8–16	8–16	8–16	8–16	8–16	8–16	8–16
9	>16	>16	>16	>16	>16	>16	>16
10	>16	>16	>16	>16	>16	>16	>16

2.3. EC measurements

Soil samples are collected and EC is measured in the laboratory considering the fact that these measurements are known to give more accurate results. In Fig. 2, the soil sample distributions are shown for the West and Southeast LUP. EC values increase towards the lake, while it has comparatively lower values towards the agricultural lands in the study areas. Unlike the West LUP, samples are collected regularly in a

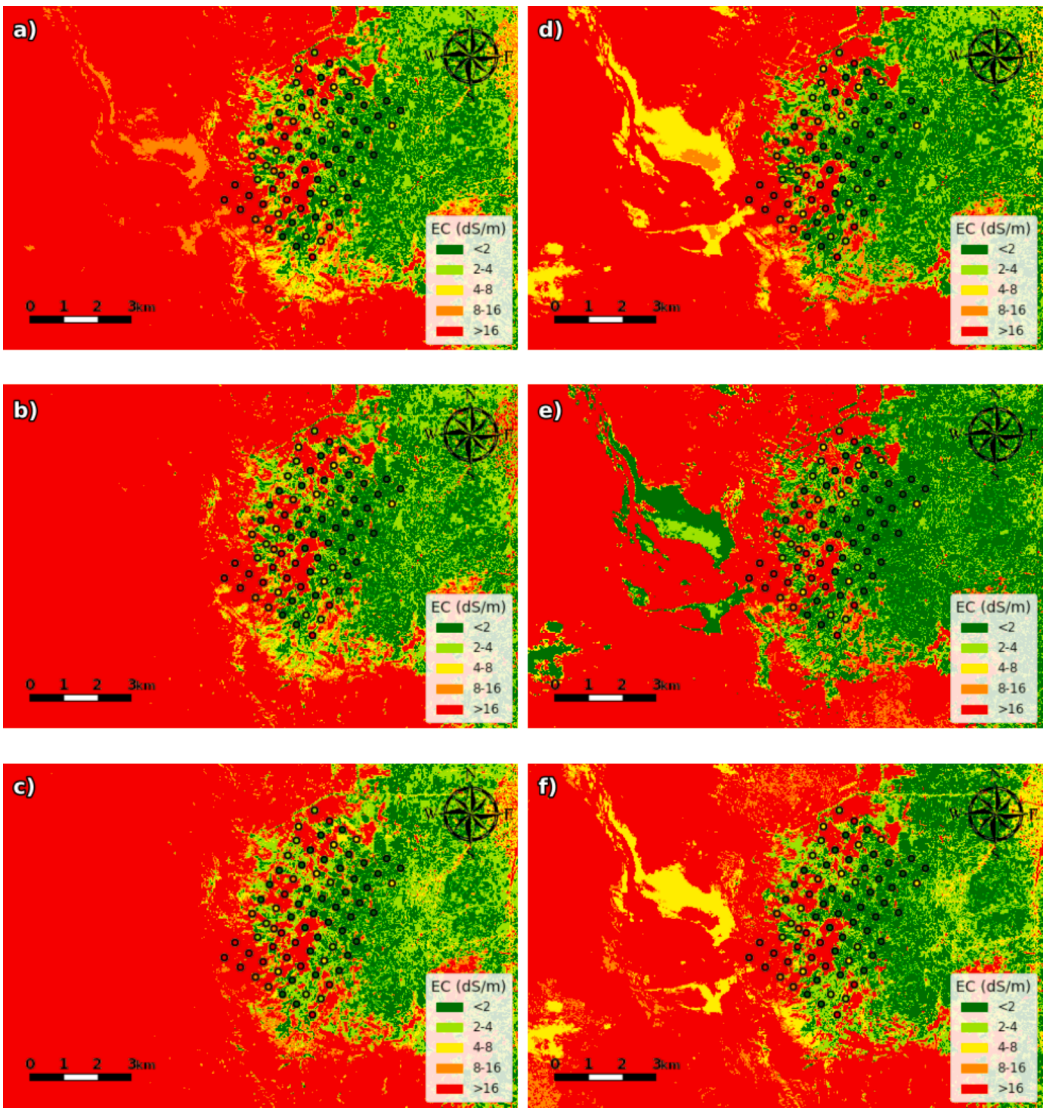

Fig. 6. The Southeast LUP Region salinity maps (a) RFR and no over-sampling, (b) RFR and ROS, (c) RFR and SMOTE, (d) XGBoost and no over-sampling, (e) XGBoost and ROS, (f) XGBoost and SMOTE.

Table 4
Accuracy results of machine learning models for the Southeast LUP Region.

Machine Learning Method	Over-sampling Method	R^2	RMSE
RFR	None	0.75	16.47
RFR	ROS	0.73	16.25
RFR	SMOTE	0.78	15.34
XGR	None	0.78	13.62
XGR	ROS	0.77	13.43
XGR	SMOTE	**0.83**	**12.24**

Table 5
Examination of salinity severity levels of the Southeast LUP test samples.

Sample	GT	RFR None	RFR ROS	RFR SMOTE	XGR None	XGR ROS	XGR SMOTE
1	0–2	0–2	2–4	2–4	0–2	0–2	0–2
2	0–2	0–2	0–2	2–4	0–2	0–2	2–4
3	0–2	4–8	8–16	4–8	0–2	0–2	0–2
4	2–4	2–4	2–4	2–4	2–4	2–4	2–4
5	2–4	2–4	2–4	4–8	2–4	2–4	2–4
6	2–4	2–4	2–4	2–4	2–4	2–4	2–4
7	4–8	4–8	4–8	4–8	4–8	4–8	4–8
8	4–8	>16	>16	>16	>16	>16	>16
9	8–16	>16	>16	>16	>16	>16	>16
10	8–16	8–16	8–16	8–16	8–16	8–16	8–16
11	>16	>16	>16	>16	>16	>16	>16
12	>16	>16	>16	>16	>16	>16	>16
13	>16	>16	>16	>16	>16	>16	>16

grid network in the Southeast LUP. However, the study area is kept wider to map salt structures. Table 1 summarizes the EC ranges and the sample counts in each salinity class obtained from the two case study areas.

3. Methodology

Initially, Landsat-8 satellite images are obtained in accordance with the collection date of the soil samples for both study areas. Features are then generated to create a model between satellite images and soil samples. The generated features are used as input for ML algorithms, while the EC data is used as the output of the model. In addition to producing maps with the trained models, these models are explained with explainable artificial intelligence (XAI) methods. Fig. 3 illustrates the methodology followed in the study.

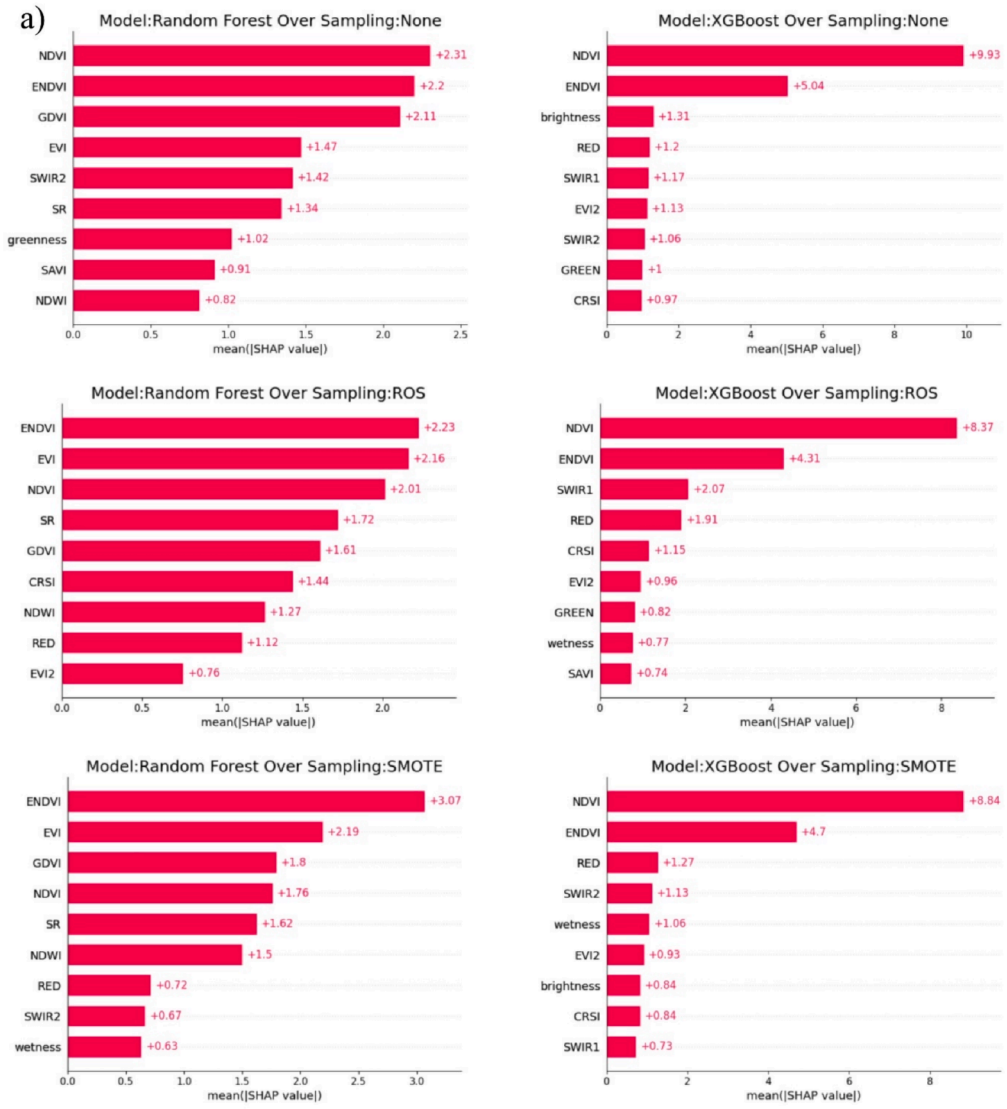

Fig. 7. Absolute SHAP values of the models developed (a) for the West, (b) Southeast LUP.

3.1. Google Earth Engine (GEE) platform

The GEE platform enables users to rapidly perform spatial analyses and visualize them with petabytes of analysis-ready spatial data. GEE allows users to achieve high-performance analyses without the need for any computing power since it is a cloud-based system. High-performance computational tools are easily available, even without high-level programming knowledge. In addition to GEE data, many spatial algorithms are offered within the framework of this platform. The platform also allows multiple people to work on the same analysis (Gorelick et al., 2017). In this study, GEE is used to produce environmental covariates calculated from different spectral bands of satellite data using 'ee.Image.expression', 'ee.Image.sampleRegions', and 'ee.Image.sampleRectangle' functions, and for the visualization of the maps using the 'ee.Image.getThumbURL' function.

3.2. Environmental covariates

Several environmental covariates are used for the estimation of soil salinity. The mechanistic model for soil development is the basement of feature determination. It is known as the SCORPAN formula (McBratney et al., 2003). The features shown in Fig. 4 are produced to determine soil, plant, and spatial characteristics in the study. Detail explanations and related references for these features could be found in (Aksoy et al., 2022) Since the topography does not change considerably in both of the study areas, it is not included in the features produced within this formula. Aksoy et al. (2022) has already assessed the performance of three ML algorithms using two different satellite platforms with the aim of suggesting the ideal set of remote sensing indices for modeling features. 26 of these features are selected for LUP and its surroundings. Moreover, a procedure named variable reduction is implemented for selecting features. In the end, five different indices have been utilized in the previous study of Aksoy et al. (2022).

3.3. Satellite image derived features

Three bands (Brightness, Greenness, and Wetness) obtained from tasseled cap transformation, original spectral bands, different vegetation, and 7 salinity indices are preferred as features in this study. Some of these indices were selected from our previous studies as they presented promising results (Gorji et al., 2020; Aksoy et al., 2022). Selected original bands are near-infrared (NIR), red, green, blue, short wave near-infrared (SWIR) one, and SWIR two bands (Aksoy et al., 2022). In total, 17 spectral indices, including 1 water index, 7 salinity indices, and 9

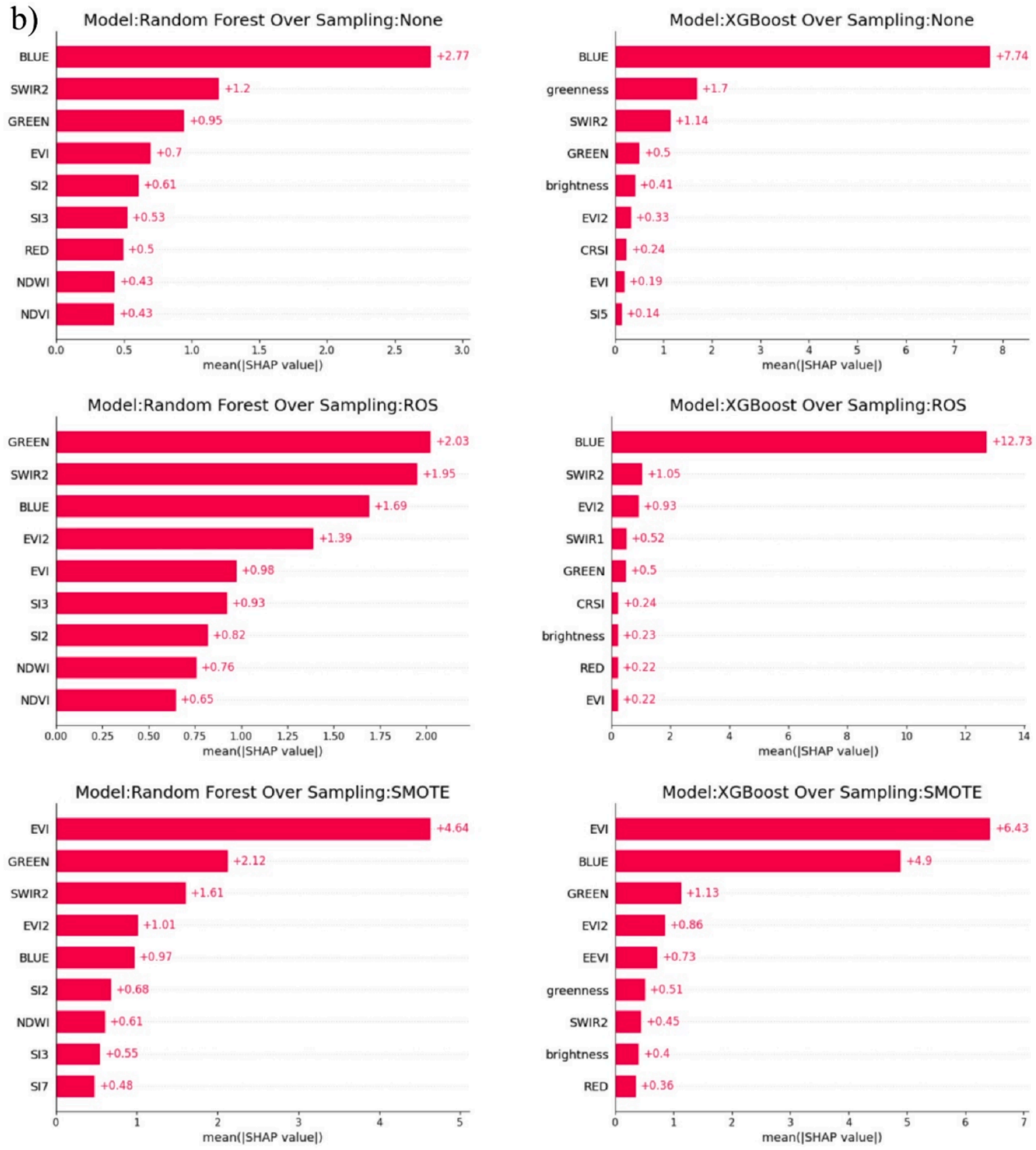

Fig. 7. (*continued*).

vegetation indices are selected. The collected 26 features are normalized to be in a range of [0,1] and are smoothed using a 3 × 3 low-pass filter (Aksoy et al., 2022).

3.4. Over-sampling techniques

Class unbalance, which leads to the dominant behavior of the majority classes, is a typical problem in ML algorithms where data sets do not have an equal or sufficient amount of samples for each class. Sampling methods can be used to correct this unstable data distribution. The goal of over-sampling techniques is to increase the data of the minority class and align it with the quantitative distribution of the majority class. Among these methods, Synthetic Minority Over-sampling Technique (SMOTE) and random over-sampling (ROS) are frequently used (Fonseca et al., 2021).

In order to obtain the sample count in the majority class, ROS is undertaken by randomly copying the data from the minority class (Hounkpatin et al., 2018). It is preferred as it is an easy method; however, it has been found that this method causes over-fitting in ML algorithms and puts forth worse results than algorithms trained without over-sampling (Fonseca et al., 2021).

The SMOTE method was introduced to literature by Chawla et al. (2002). Instead of randomly replicating a minority of samples, this method creates unit vectors between neighboring samples determined

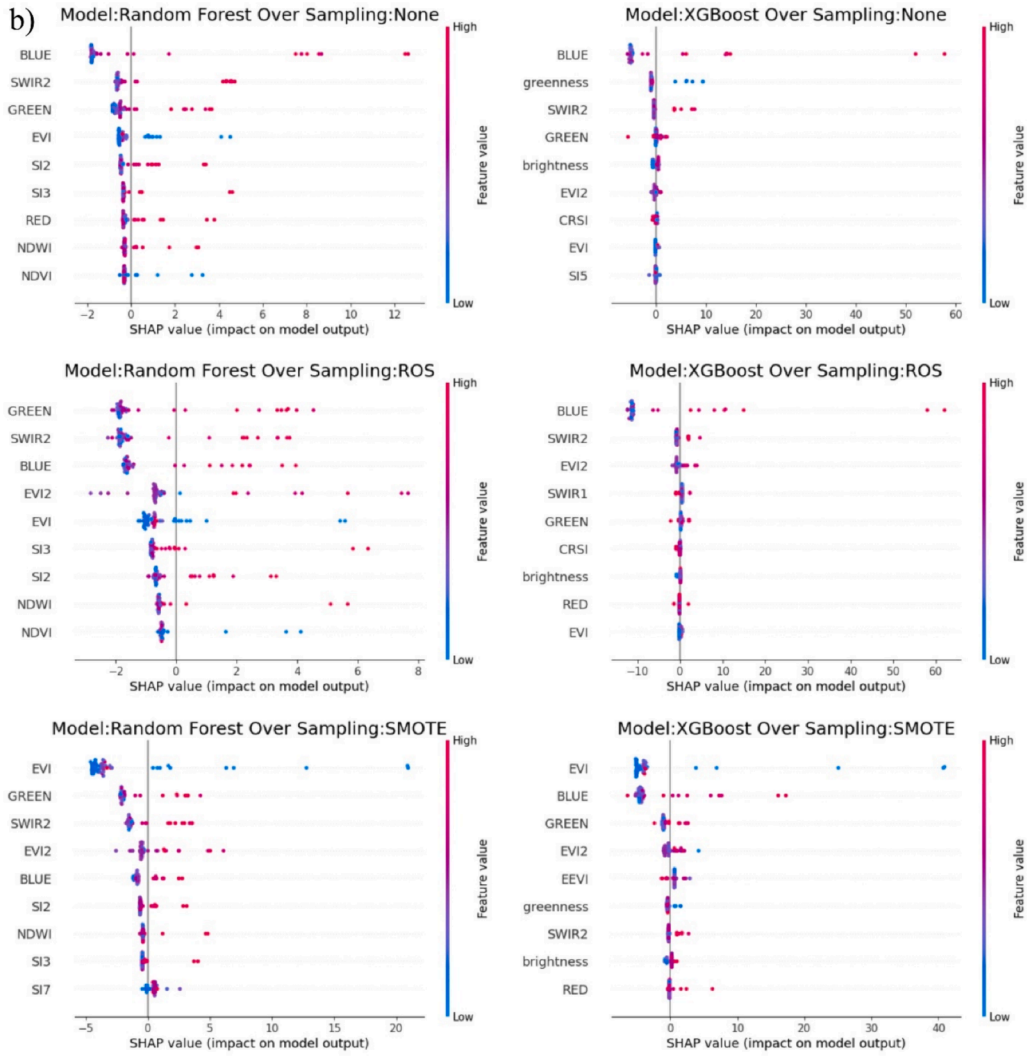

Fig. 8. SHAP summary graphs for (a) West and (b) Southeast LUP.

by the nearest neighbor method. This vector is then rescaled by a random number from 0 to 1 to represent a new point in the feature space. This new point is synthetically generated.

We have applied ROS and SMOTE over-sampling methods to the samples falling into five salinity classes by adding the aforementioned characteristics. We then trained the ML algorithms with the original reference data (without over-sampling) and with the new reference data generated from over-sampling methods.

3.5. ML approaches

Breiman (2001) introduced the Random Forest (RF) ML technique. The classification and regression tree algorithm is the foundation of this ensemble learning strategy. Decision trees that are by themselves a weak ML method are combined to form a powerful ensemble ML algorithm (Wang et al., 2019). RF algorithm provides solutions to both regression and classification problems (Li et al., 2019). RF implemented using Sklearn Python library, which was developed by (Pedregosa et al., 2011).

One of the quickest gradient-boosting tree algorithms is called eXtreme Gradient Boosting (XGBoost) introduced by Chen and Guestrin (2016) in Python. It achieves its computational efficiency by overcoming an important shortcoming of gradient-boosted trees. When creating a new split for the tree, potential errors are estimated for all previous member splits.

XGBoost addresses this shortcoming by examining the distribution of all data points in the leaf of the tree, narrowing the space in which it searches for feature separation. Although various regularization methods work within XGBoost, it is fast and convenient, and many hyperparameter possibilities can be found quickly. XGBoost also offers regularization to prevent overfitting (Zarei et al., 2021). The overall architecture of XGBoost is similar to the RF algorithm, but the trees are not as independent in parallel as in the RF algorithm.

3.6. Explainable artificial intelligence (XAI)

XAI methods are algorithms designed to explain the behavior of ML algorithms expressed as black boxes (Stadtler et al., 2022). Various XAI methods have been presented in the literature. Among them, perturbation-based methods such as Shapley Additive Explanations (SHAP) and Local Interpretable Model-agnostic Explanations (LIME), and gradient-based methods such as Learning Important FeaTures (DeepLIFT), SmoothGrad, and Gradient-weighted Class Activation Mapping (GradCAM) can be addressed (Krishna et al., 2022). These methods can be utilized to explain ML, however, picking a method and relying on its results is tricky. The problem with explanations is the importance of the features changing from one XAI method to another. This problem is known as Rashomon Effect in literature (Baniecki et al.,

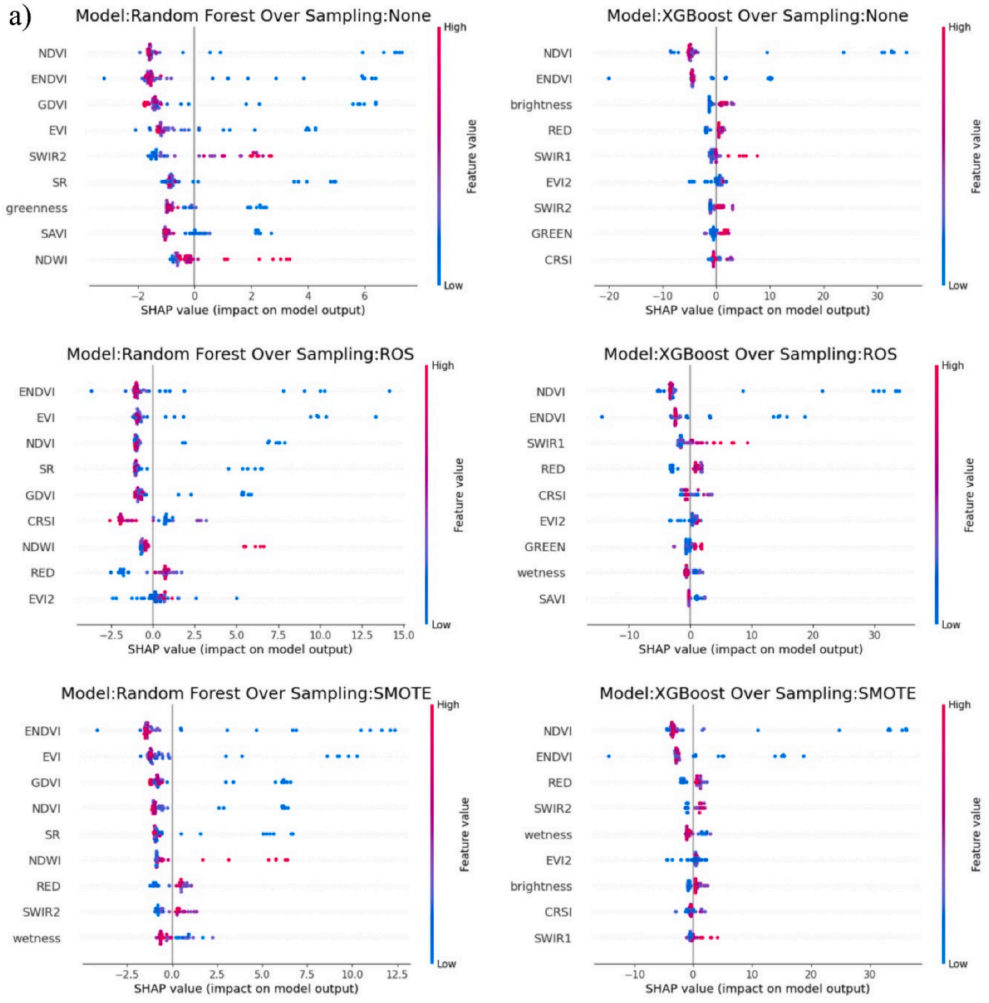

Fig. 8. (*continued*).

2023). According to Breiman (2001), slight changes in data and models can affect explanations substantially. Ensemble models are especially prone to this effect since a slight disturbance in the model or data results in skipping from one model to another. Krishna et al. (2022) focused on the multiplicity problem of XAI and found that SHAP is the most preferred algorithm in the case of the Rashomon Effect.

3.6.1. *Shapley additive explanations (SHAP)*

SHAP was first introduced by Lundberg and Lee (2017). Its values can be derived for any model since they are independent of the model. Permutation sampling approximation is used under the assumption of feature independence. Values are essentially model feature contributions. The base value is the model's expected result. The contribution of SHAP values to the model indicates how far the model moves away from this base value. Features that contribute more are considered as features that are important for the model. Both negative and positive contributions are possible. Absolute SHAP values represent the significance of the characteristics, whereas the average of the absolute SHAP values over all outcomes reflects the significance of the features as a whole (Stadtler et al., 2022). Analyses in this study with the SHAP method are presented in 4 graphs, namely summary, feature importance, dependency, and force graphs.

For each training sample, the SHAP summary graph illustrates the influence of the model input features on the model output. It is colored according to the values of the inputs and presents the values of the inputs that contribute to the model. The SHAP feature importance graph shows the joint absolute contribution as a bar graph instead of the contribution of each data shown in the summary graph. This graph highlights the total contribution to the model. The direction in which it contributes to the model is ignored. The dependency graph explains the relationship between two features in the model. It explains the contribution of a feature to the model through both the value of that feature and the value of another feature that is dependent on that feature. A force plot is a graph showing each feature's contribution to the model for a single sample. It expresses the base value estimated for the regression model and the contribution of the features of the selected sample to the model, together with the model output at the end of the summation.

3.7. *Accuracy assessment*

Root mean square error (RMSE) and coefficient of determination (R^2) metrics are used to calculate the accuracy of the test samples. RMSE and R^2 are expressed in equations (1) and (2) (Wang et al., 2019).

$$RMSE = \sqrt{\frac{1}{n}\sum_{i=1}^{n}(X_i - Y_i)^2} \tag{1}$$

$$R^2 = 1 - \frac{\sum_{i=1}^{n}(X_i - Y_i)^2}{\sum_{i=1}^{n}(X_i - \underline{X})^2} \tag{2}$$

where n stands for the sample count, Xi for the observed soil salinity, Yi for the estimated soil salinity, and X for the average measured salinity value.

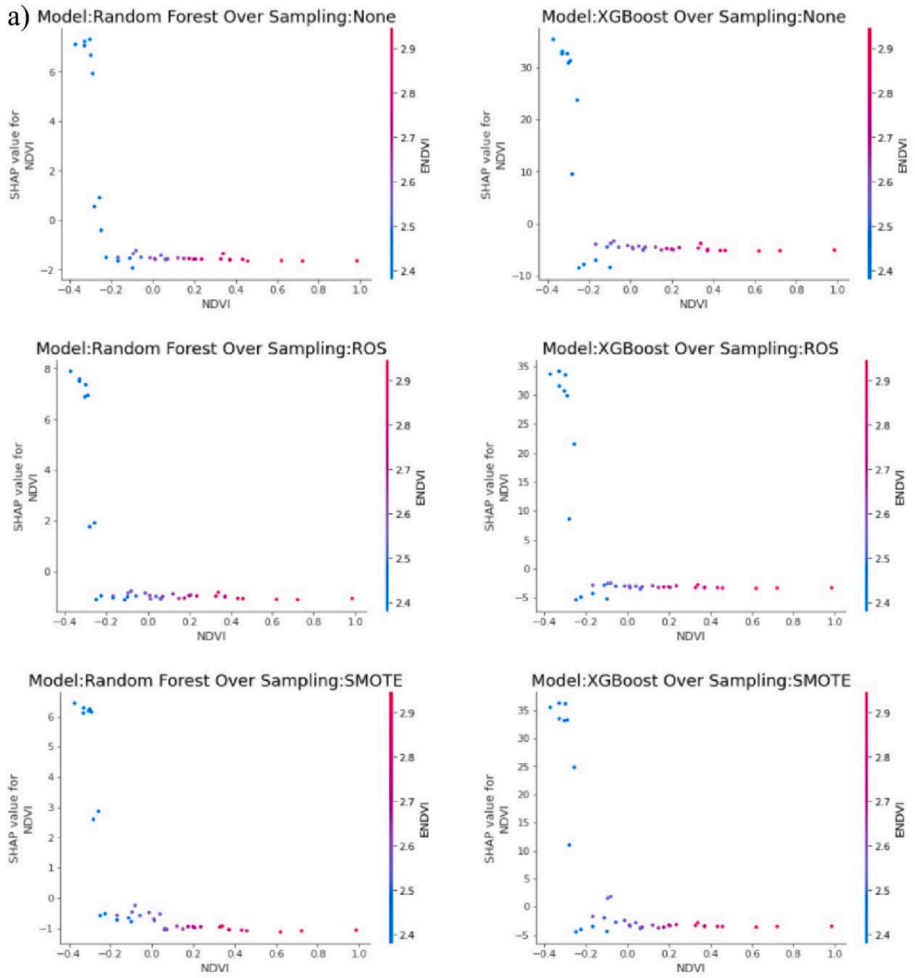

Fig. 9. Dependency plots of Blue and EVI feature in the (a) West, and (b) Southeast LUP. (For interpretation of the references to color in this figure legend, the reader is referred to the web version of this article.)

4. Results

We have generated soil salinity maps for 6 scenarios. These scenario combinations are produced by combining 2 ML algorithms with 3 different sampling cases. While we have used RF and XGBoost as ML algorithms; we have generated 3 different sampling cases, one with original data and new data formed by over-sampling with ROS and SMOTE methods. In summary, the following model and data combinations are created and tested:

- Test 1: RF model and original data,
- Test 2: RF model and data generated by ROS,
- Test 3: RF model and data generated with SMOTE,
- Test 4: XGBoost model and original data,
- Test 5: XGBoost model and data generated by ROS,
- Test 6: XGBoost model and data generated with SMOTE.

We have conducted our initial assessments on the visual interpretation of the soil salinity maps by domain experts. We have also evaluated the training and test performance of models. Afterwards, summary, importance, dependency, and force plots have been produced using the SHAP method to validate and explain the models produced as a result of the determined tests.

4.1. West LUP model accuracies and salinity maps

Soil salinity maps for the West LUP are shown in Fig. 5. Both ML models are able to identify areas close to the lake as extremely saline. However, the RF algorithm identified some specific regions far from the lake as highly saline, as can be observed in Fig. 5 (a), (b), and (c). These regions are either villages and factories or uncultivated lands. Although these areas are slightly or non-saline, they are incorrectly predicted by the regression analysis as they are not cultivated. When Fig. 5 (d), (e), and (f) are examined, it is clear that XGBoost model has produced more consistent maps. However, the red pixels within agricultural lands are uncultivated lands with around 4–8 dS/m. The soil salinity map generated from XGBoost-SMOTE (Fig. 5(f)) better represents the salinity conditions compared to the XGBoost-no oversampling experiment Fig. 5 (d). Considering the outcomes of the previous studies in this field conducted by Aksoy et al. (2022), the XGBoost algorithm achieved more accurate results. This visually determined accuracy is also reflected in the statistical analysis. As shown in Table 2, R^2 values are higher for the XGBoost compared to the RF algorithm, while RMSE values are comparatively lower. The XGBoost-ROS experiment yielded the lowest RMSE and the highest R2 values. Upon comparing the RMSE values, it was observed that the RFR none and RFR SMOTE methods demonstrated similar performance. Conversely, the disparity in RMSE between RFR-ROS and XGR-ROS was 2.3, favoring the XGBoost approach. The salinity levels of 10 test samples after regression are shown in Table 3. It

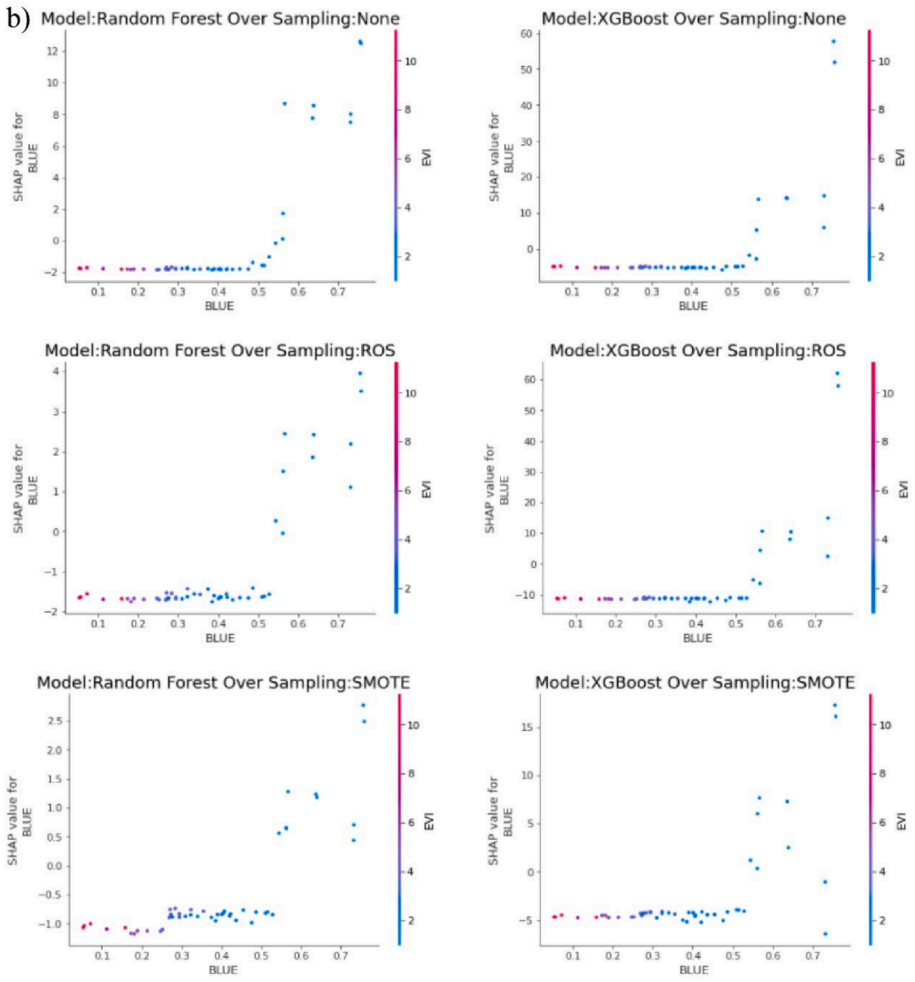

Fig. 9. (*continued*).

is seen that the XGBoost algorithm gives a more accurate result with samples falling in the same or close to the same class.

4.2. Southeast LUP model accuracies and salinity maps

The salinity maps produced for the Southeast LUP are illustrated in Fig. 6. The RF algorithm effectively delineates the saline lands proximate to the lake as highly saline, whereas XGBoost classifies this region as ranging from non-saline to moderately saline. However, it is anticipated that this area will exhibit highly saline characteristics. Conversely, the XGBoost-ROS method categorizes this region as non-saline. Given that soil salinity is typically low in agricultural areas, it is noteworthy that all models have identified these areas as slightly saline or non-saline, representing a significant finding. When the accuracy results for the Southeast LUP shown in Table 4 were analyzed, the XGBoost model provided better results than the RF model, and the best R^2 and minimum RMSE values were obtained with the XGR-SMOTE approach. However, the difference in RMSE between RFR ROS and RFR SMOTE is 1.19. Visual analysis in areas other than salt structures is consistent with these findings. When the test samples shown in Table 5 are evaluated, it is concluded that the XGBoost algorithm performed better on non-saline samples.

4.3. Explainable ML results

We have performed a SHAP analysis of the ML models in 4 stages: Initially, each feature's absolute contribution to the model outcome is examined. Secondly, the direction in which the features contribute to the model and how their values contribute to the model are investigated. Thirdly, the dependency between the two most contributing features is examined in the model. Finally, the contributions of the features to the models are scrutinized on a sample-by-sample based on the test samples selected from both domains demonstrated in Table 4 and Table 5.

Absolute SHAP values for the West and Southeast LUP are shown in Fig. 6. It can be seen that plant status-related indices like ENDVI, NDVI, and EVI highly contribute to the model output, as seen in Fig. 7(a). Similar to the previous study of Aksoy et al. (2022), it is clear that the CRSI index also highly contributes to the model in this area. Fig. 7(b) shows that the blue and green bands are the features that contribute most to the model. Vegetation indices also contributed to the model, although not as much as the West LUP.

The input of SHAP values and features to the model can be seen as positive and negative. Their effect on the model according to the features of the West and Southeast LUP is shown in Fig. 8. When the features of the model are analyzed in Fig. 8(a), it can be stated that high values of indices such as ENDVI and NDVI contribute to low a expectancy of salinity, while low values contribute to high levels of salinity. NDWI index provided the opposite contribution. The conclusion to be drawn from these findings is that with increasing soil salinity, vegetation cover decreases. In Fig. 8(b), low values of the bands, such as those in blue and green, contribute to the soil's low salinity severity, whereas high values contribute to the soil's high salinity level. Based on these findings, it can be concluded that saline areas are brighter areas in the visible region. Therefore, salt crusts can easily be distinguished on

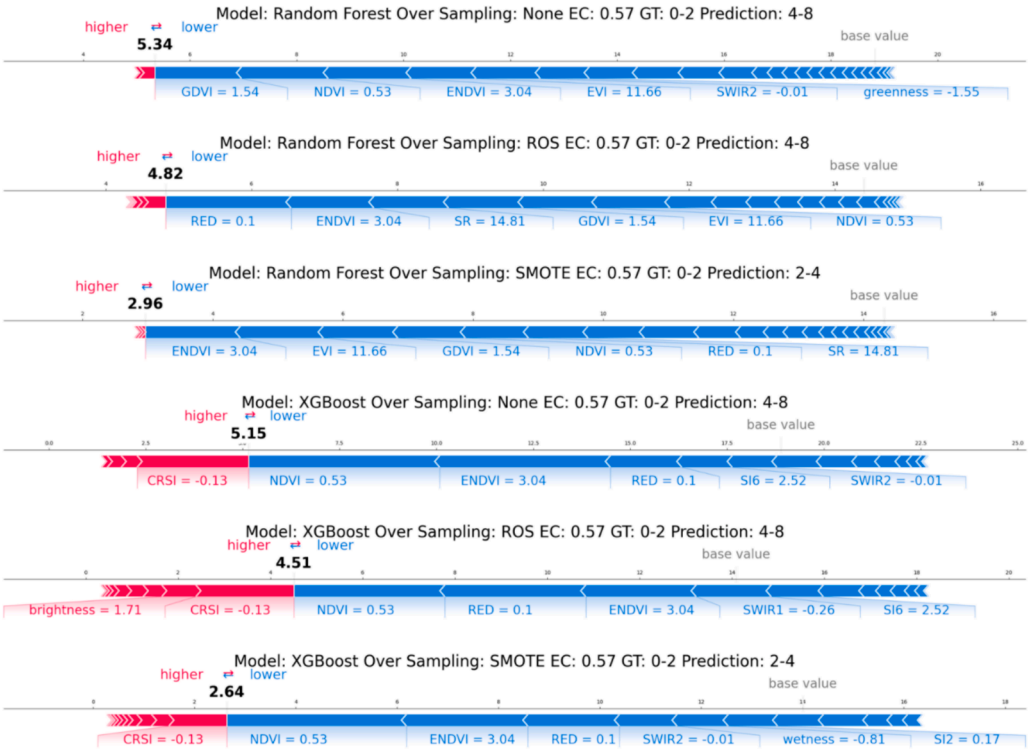

Fig. 10. West LUP 1st test sample force plot.

Fig. 11. West LUP 3rd test sample force plot.

satellite images by being white and bright.

The two most contributing features among the 6 tests are compared in terms of dependency. NDVI and ENDVI features are analyzed in the dependency graph created for the West LUP, as shown in Fig. 9(a). When the graph is analyzed, it is seen that low values of both NDVI and ENDVI features positively contribute to the model. This result is independent of the model and over-sampling methods. The reason is that NDVI and ENDVI features are mostly produced by combining the same features. In Fig. 9(b), unlike the West LUP, blue and EVI features contributed the most to this region. Thus, the dependency between these two features is

Fig. 12. West LUP 10th test sample force plot.

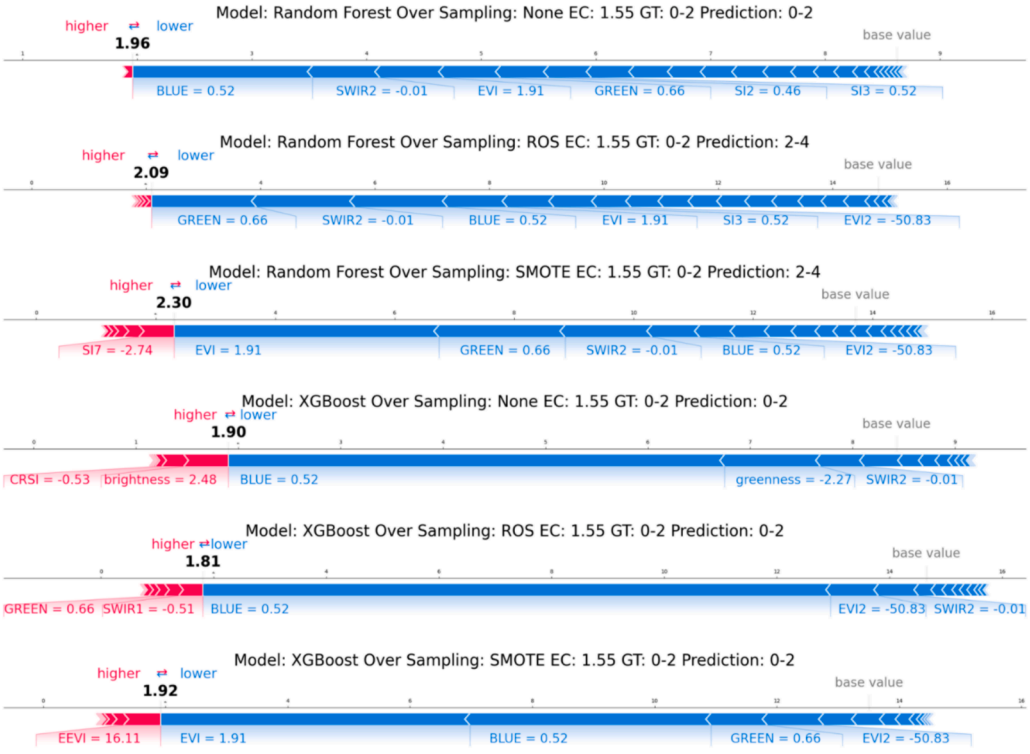

Fig. 13. Southeast LUP Region 1st test sample force plot.

Fig. 14. Southeast LUP Region 8th test sample force plot.

Fig. 15. Southeast LUP Region 12th test sample force plot.

analyzed. It is observed that the low values of the blue band contribute negatively to the model, while the low values of EVI contribute positively. An inverse correlation between these two features is common to all models and over-sampling tests. The blue feature of the model shifts towards positive, especially for values higher than 0.55.

In order to explain the models on the basis of test samples, SHAP force plots for the West LUP are analyzed in Figs. 10–12. The characteristic results mirror the findings of the overall analysis. The graphs basically describe EC values that each feature adds or subtracts from a base value, which is the value predicted by the model without using any features. When the 10 samples tested for the West LUP are analyzed, it is found that indices such as ENDVI and NDVI had a decreasing effect on

the regression result, except for extremely saline samples.

When the test sample shown in Fig. 10 is examined, it is understood that the model obtained with the XGBoost algorithm and SMOTE over-sampling method finds the closest value to the real situation. The model predicted the value of 0.57 dS/m as 2.64 dS/m. The NDVI value of 0.53 and the ENDVI value of 3.04 provided the most negative contribution to the model result, while CRSI offered a positive contribution with a value of −0.13.

The 3rd test sample force plot is shown in Fig. 11. When this force plot is investigated, none of the models are able to predict the correct salinity level. The closest models are the XGBoost and SMOTE over-sampling method. While NDVI and EVI2 features performed the most negative contribution, SI6, which is one of the salinity indices, made the most positive contribution to the model.

The force plots for the 10th test sample, which is the last trial for the West LUP, are shown in Fig. 12. Although all models give different results from the actual EC values, the closest result is given by the XGBoost algorithm with the ROS over-sampling method, with a value of 37.56 dS/m. However, all models still predicted values within the correct salinity level. ENDVI and green features made the most positive contribution, while NDVI made a negative contribution in this test.

The graphs produced for the 13 test samples selected for the Southeast LUP Region are shown in Figs. 13–15. The blue band contributes negatively to the regression of soil salinity, while the green band contributes in direct proportion to the salinity level. Salinity indices contribute positively, especially as salinity increases. The brightness value contributes positively to the regression result at most salinity levels.

Fig. 13 shows the force plots for the 1st test sample in the Southeast LUP Region. The model that exerted the closest prediction is the XGBoost and ROS over-sampling method, with a value of 1.81 dS/m. Green and SWIR1 features positively contribute to the model, while blue and EVI2 features are the most negative contributors.

When the force plots of the 8th test sample shown in Fig. 14 are analyzed, it is seen that none of the models made a prediction close to reality. The closest estimate is obtained by the XGBoost algorithm with a value of 24.16 dS/m with the SMOTE over-sampling method. The EVI feature contributes negatively, whereas both blue and green features positively contribute to the model result.

The force graphs shown in Fig. 15 belong to the 12th test. When these graphs are analyzed, it is noticeable that the XGBoost algorithm predicts notably closer results. The XGBoost model, with a value of 31.27 dS/m, is the model that offered the most accurate prediction. The blue and green features have the most positive contribution, while the EVI2 feature has the most negative contribution to the model result.

A comparison of methods developed for soil salinity prediction indicates that ML methods exert better results than simpler methods such as linear regression. Despite the limited availability of local samples, ML algorithms can still perform good predictions. In particular, the XGboost algorithm achieved higher accuracy results than the RF algorithm. It only had difficulty detecting the salt crust in the Southeast LUP Region, which represents extremely saline soil. The SMOTE over-sampling method also contributes the most to the accuracy of the ML models.

5. Discussion

Similar studies investigated ML performance on this phenomenon. They also found that ML models are capable of predicting soil salinity with high accuracy, as further discussed below.

Considering the former study of Aksoy et al. (2022) for the same region, lower accuracy is obtained for the West LUP. The reason for this may be attributed to varying local samples, satellite imagery with different dates, and accuracy analysis with cross-validation.

Zarei et al. (2021) compared the XGBoost method with RF in the study of soil salinity with ML methods. They conducted the study in the Eshtehard City of Iran. Similar to the results of this study, XGBoost predicted the best result with an R^2 value of 0.76 in determining soil salinity, where the model was trained using 46 features.

Zhou et al. (2022) compared RF and XGBoost ML algorithms in their global salinity studies. Similar to this study, they found out that the XGBoost algorithm gave the best result. This method reached the best result with R^2 of 0.71, followed by the RF algorithm with R^2 of 0.69.

Another study comparing XGBoost, RF, and decision trees in modeling soil salinity was conducted by Ma et al. (2021). The study worked with soil samples collected in 2018 in the Tarim Basin of China. The XGBoost method gave a better result than RF with a difference of 5 %.

Similar studies by Ma et al. (2021) and Zhou et al. (2022) searched the feature importance ratings produced by the XGBoost algorithm to analyze the contribution of features to the models. Feature importance graphs were similar to SHAP feature importance graphs. However, SHAP was able to explain not only the importance of features, but also the direction in which they contributed to the model, both for the overall model and on a sample basis. The dependencies between features were expressed as correlations in these recent studies. SHAP also provides the opportunity to examine the dependencies of features according to their contribution to the model.

The soil salinity mapping results may exhibit substantial variation across diverse environmental contexts. Given that numerous other physical attributes, including color, texture, and moisture, can influence the surface reflectance of saline soils, the exclusive reliance on a singular feature may not consistently yield precise estimates in all cases (Daliakopoulos et al., 2016).

6. Conclusions and recommendations

Soil salinity should be recognized as a significant problem by decision-makers and prevention measures should be taken before it causes more critical issues, such as food crises. As used in the identification of many environmental problems, RS and ML methods play important roles in the determination and monitoring of soil salinity. Therefore, in the scope of the United Nations Sustainable Development Goals, we suggest periodic monitoring of soil salinity using RS-based systems and ML methods to provide reliable information to take necessary interventions within the nexus of food security-water use-sustainability (UN, 2022).

It has always been a matter of debate whether ML algorithms are a closed box and whether the decisions they make are based on the right reasons. XAI methods have brought a solution to this problem. Since SHAP values have been frequently used in literature, their use is also preferred in this study. SHAP values have revealed how soil salinity is affected and by which characteristics within the scope of the study. The identification of important features can exhibit significant variability across different model configurations, as indicated by SHAP explanations. This underscores the necessity for further research on the interpretability of machine learning models in the context of soil salinity mapping.

Lake Urmia Basin is economically and ecologically important in the northwest of Iran. However, due to human impact and excessive use of groundwater, the problem of soil salinization in agricultural lands has been emerging over time. This problem adversely affects agricultural activities. Soil salinity, which has highly increased in recent years, has become critical to the point of abandonment of agricultural lands. Therefore, it is a significant problem to detect, monitor, and intervene in soil salinity in this region.

The findings of this study demonstrate that while the XGBoost ML algorithm produces superior outcomes, it has difficulty in capturing the extremely saline salt crusts in the Southeast LUP Region. Data diversification methods improve model accuracy. In terms of SHAP values, although different for the two study areas, visible and near-infrared bands, as well as the vegetation indices derived from them, are found to make high contributions to the models. In conclusion, visible bands

are related to soil salinity in a way that a brighter surface has a comparatively high level of salinity. Especially surfaces like salt crust are considered highly bright with high salinity values. In addition to the brightness effect, vegetation is also heavily influenced by soil salinity. As such, a lack of vegetation and resulting changes in vegetation indices have a remarkable effect. Physical properties of saline soil, such as brightness and effects on vegetation, are also shown as important features for soil salinity modeling by SHAP explanations.

The limitation of taking this study further is the limited availability of ground measurements. ML methods are ultimately trained with the available data. It is obvious that when models are trained and tested with more data, they will produce more reliable results. The quality of the data collection for soil salinity can also be increased by choosing possible areas via satellite before collecting field samples.

CRediT authorship contribution statement

Samet Aksoy: Data curation, Investigation, Methodology, Software, Validation, Visualization, Writing – original draft. **Elif Sertel:** Conceptualization, Methodology, Resources, Supervision, Validation, Writing – original draft, Writing – review & editing. **Ribana Roscher:** Methodology, Writing – review & editing. **Aysegul Tanik:** Conceptualization, Validation, Writing – review & editing. **Nikou Hamzehpour:** Resources, Validation, Writing – review & editing.

Declaration of competing interest

The authors declare that they have no known competing financial interests or personal relationships that could have appeared to influence the work reported in this paper.

Data availability

Soil salinity maps and field data are provided upon justifiable request from the corresponding author.

Acknowledgements

The authors would like to thank the Office of the Dean of Research and Scientific Research Unit of Istanbul Technical University for the funding support. This work has been partially funded by the Deutsche Forschungsgemeinschaft (DFG, German Research Foundation) under Germany's Excellence Strategy, EXC-2070-3390732324-PhenoRob.

References

Akca, S., Gungor, O., 2022. Semantic segmentation of soil salinity using in-situ EC measurements and deep learning based U-NET architecture. Catena 218, 106529. https://doi.org/10.1016/j.catena.2022.106529.

Aksoy, S., Yildirim, A., Gorji, T., Hamzehpour, N., Tanik, A., Sertel, E., 2022. Assessing the performance of machine learning algorithms for soil salinity mapping in Google Earth Engine platform using Sentinel-2A and Landsat-8 OLI data. Adv. Space Res. 69, 1072–1086. https://doi.org/10.1016/j.asr.2021.10.024.

Allbed, A., Kumar, L., 2013. Soil salinity mapping and monitoring in arid and semi-arid regions using remote sensing technology: a review. Adv. Remote Sens. 2013 https://doi.org/10.4236/ars.2013.24040.

Baniecki, H., Parzych, D., Biecek, P., 2023. The grammar of interactive explanatory model analysis. Data Min. Knowl. Disc. https://doi.org/10.1007/s10618-023-00924-w.

Breiman, L., 2001. Random Forests. Mach. Learn. 45, 5–32. https://doi.org/10.1023/A:1010933404324.

Brevik, E.C., Cerdà, A., Mataix-Solera, J., Pereg, L., Quinton, J.N., Six, J., Van Oost, K., 2015. The interdisciplinary nature of SOIL. SOIL 1, 117–129. https://doi.org/10.5194/soil-1-117-2015.

Chawla, N.V., Bowyer, K.W., Hall, L.O., Kegelmeyer, W.P., 2002. SMOTE: synthetic minority over-sampling technique. J. Artif. Intell. Res. 16, 321–357. https://doi.org/10.1613/jair.953.

Chen, T., Guestrin, C., 2016. XGBoost: a scalable tree boosting system. In: Proceedings of the 22nd ACM SIGKDD International Conference on Knowledge Discovery and Data Mining, pp. 785–794. https://doi.org/10.1145/2939672.2939785.

Chen, H., Ma, Y., Zhu, A., Wang, Z., Zhao, G., Wei, Y., 2021. Soil salinity inversion based on differentiated fusion of satellite image and ground spectra. Int. J. Appl. Earth Observ. Geoinf. 101, 102360 https://doi.org/10.1016/j.jag.2021.102360.

Daliakopoulos, I.N., Tsanis, I.K., Koutroulis, A., Kourgialas, N.N., Varouchakis, A.E., Karatzas, G.P., Ritsema, C.J., 2016. The threat of soil salinity: a European scale review. Sci. Total Environ. 573, 727–739. https://doi.org/10.1016/j.scitotenv.2016.08.177.

Fonseca, J., Douzas, G., Bacao, F., 2021. Improving imbalanced land cover classification with K-means SMOTE: detecting and oversampling distinctive minority spectral signatures. Information 12, 266. https://doi.org/10.3390/info12070266.

FAO, 2023. GSASmap | Global Soil Partnership | Food and Agriculture Organization of the United Nations [WWW Document]. URL https://www.fao.org/global-soil-partnership/gsasmap/en (accessed 1.31.23).

Garajeh, M.K., Malakyar, F., Weng, Q., Feizizadeh, B., Blaschke, T., Lakes, T., 2021. An automated deep learning convolutional neural network algorithm applied for soil salinity distribution mapping in Lake Urmia, Iran. Sci. Total Environ. 778, 146253 https://doi.org/10.1016/j.scitotenv.2021.146253.

Ge, X., Ding, J., Teng, D., Xie, B., Zhang, X., Wang, J., Han, L., Bao, Q., Wang, J., 2022. Exploring the capability of Gaofen-5 hyperspectral data for assessing soil salinity risks. Int. J. Appl. Earth Observ. Geoinf. 112, 102969 https://doi.org/10.1016/j.jag.2022.102969.

Gorelick, N., Hancher, M., Dixon, M., Ilyushchenko, S., Thau, D., Moore, R., 2017. Google Earth Engine: planetary-scale geospatial analysis for everyone. Remote Sens. Environ. Big Remotely Sensed Data: Tools Appl. Exp. 202, 18–27. https://doi.org/10.1016/j.rse.2017.06.031.

Gorji, T., Yildirim, A., Hamzehpour, N., Tanik, A., Sertel, E., 2020. Soil salinity analysis of Urmia Lake Basin using Landsat-8 OLI and Sentinel-2A based spectral indices and electrical conductivity measurements. Ecol. Ind. 112, 106173 https://doi.org/10.1016/j.ecolind.2020.106173.

Gu, Q., Han, Y., Xu, Y., Ge, H., Li, X., 2022. Extraction of saline soil distributions using different salinity indices and deep neural networks. Remote Sens. (Basel) 14, 4647. https://doi.org/10.3390/rs14184647.

Haghighi, A., Fazel, N., Hekmatzadeh, A.A., Klöve, B., 2018. Analysis of effective environmental flow release strategies for Lake Urmia Restoration. Water Resour. Manage. 32, 3595–3609. https://doi.org/10.1007/s11269-018-2008-3.

Hamzehpour, N., Eghbal, M.K., Abasiyan, S.M.A., Dill, H.G., 2018. Pedogenic evidence of Urmia Lake's maximum expansion in the late Quaternary. Catena 171, 398–415. https://doi.org/10.1016/j.catena.2018.07.019.

Hamzehpour, N., Marcolli, C., Pashai, S., Klumpp, K., Peter, T., 2022. Measurement report: The Urmia playa as a source of airborne dust and ice-nucleating particles – Part 1: correlation between soils and airborne samples. Atmos. Chem. Phys. 22, 14905–14930. https://doi.org/10.5194/acp-22-14905-2022.

Hounkpatin, K.O.L., Schmidt, K., Stumpf, F., Forkuor, G., Behrens, T., Scholten, T., Amelung, W., Welp, G., 2018. Predicting reference soil groups using legacy data: a data pruning and Random Forest approach for tropical environment (Dano catchment, Burkina Faso). Sci. Rep. 8, 9959. https://doi.org/10.1038/s41598-018-28244-w.

Kabiraj, S., Jayanthi, M., Vijayakumar, S., Duraisamy, M., 2022. Comparative assessment of satellite images spectral characteristics in identifying the different levels of soil salinization using machine learning techniques in Google Earth Engine. EarthSci Inform. https://doi.org/10.1007/s12145-022-00866-9.

Krishna, S., Han, T., Gu, A., Pombra, J., Jabbari, S., Wu, S., Lakkaraju, H., 2022. The Disagreement Problem in Explainable Machine Learning: A Practitioner's Perspective. doi: 10.48550/arXiv.2202.01602.

Li, Z., Li, Y., Xing, A., Zhuo, Z., Zhang, S., Zhang, Y., Huang, Y., 2019. Spatial prediction of soil salinity in a semiarid oasis: environmental sensitive variable selection and model comparison. Chin. Geogr. Sci. 29, 784–797. https://doi.org/10.1007/s11769-019-1071-x.

Lundberg, S.M., Lee, S.-I., 2017. A unified approach to interpreting model predictions. In: Advances in Neural Information Processing Systems. Curran Associates, Inc.

Ma, G., Ding, J., Han, L., Zhang, Z., Ran, S., 2021. Digital mapping of soil salinization based on Sentinel-1 and Sentinel-2 data combined with machine learning algorithms. Reg. Sustain. 2, 177–188. https://doi.org/10.1016/j.regsus.2021.06.001.

Ma, S., He, B., Xie, B., et al., 2023. Investigation of the spatial and temporal variation of soil salinity using Google Earth Engine: a case study at Werigan-Kuqa Oasis, West China. Sci. Rep. 13, 2754. https://doi.org/10.1038/s41598-023-27760-8.

Marcus, G., 2018. Deep learning: a critical appraisal. Comput. Sci. https://doi.org/10.48550/arXiv.1801.00631.

Masoud, A.A., Koike, K., Atwia, M.G., El-Horiny, M.M., Gemail, K.S., 2019. Mapping soil salinity using spectral mixture analysis of landsat 8 OLI images to identify factors influencing salinization in an arid region. Int. J. Appl. Earth Observ. Geoinf. 83, 101944 https://doi.org/10.1016/j.jag.2019.101944.

McBratney, A.B., Mendonça Santos, M.L., Minasny, B., 2003. On digital soil mapping. Geoderma 117, 3–52. https://doi.org/10.1016/S0016-7061(03)00223-4.

Mohammadifar, A., Gholami, H., Golzari, S., Collins, A.L., 2021. Spatial modelling of soil salinity: deep or shallow learning models? Environ. Sci. Pollut. Res. 28, 39432–39450. https://doi.org/10.1007/s11356-021-13503-7.

Mohammadifar, A., Gholami, H., Golzari, S., 2022. Assessment of the uncertainty and interpretability of deep learning models for mapping soil salinity using DeepQuantreg and game theory. Sci. Rep. 12, 15167. https://doi.org/10.1038/s41598-022-19357-4.

Motaghi, F., Hamzehpour, N., Mola Ali Abasiyan, S., Rahmati, M., 2020. The wind erodibility in the newly emerged surfaces of Urmia Playa Lake and adjacent agricultural lands and its determining factors. CATENA 194, 104675. https://doi.org/10.1016/j.catena.2020.104675.

Pedregosa, F., Varoquaux, G., Gramfort, A., Michel, V., Thirion, B., Grisel, O., Blondel, M., Prettenhofer, P., Weiss, R., Dubourg, V., Vanderplas, J., Passos, A., Cournapeau, D., 2011. Scikit-learn: machine learning in Python. J. Mach. Learn. Res. 6.

Sahbeni, G., Ngabire, M., Musyimi, P.K., Székely, B., 2023. Challenges and opportunities in remote sensing for soil salinization mapping and monitoring: a review. Remote Sens. (Basel) 15, 2540. https://doi.org/10.3390/rs15102540.

Stadtler, S., Betancourt, C., Roscher, R., 2022. Explainable machine learning reveals capabilities, redundancy, and limitations of a geospatial air quality benchmark dataset. Mach. Learn. Knowl Extract. 4, 150–171. https://doi.org/10.3390/make4010008.

Stavi, I., Thevs, N., Priori, S., 2021. Soil salinity and sodicity in drylands: a review of causes, effects, monitoring, and restoration measures. Front. Environ. Sci. 9.

Taghizadeh, R., Schmidt, K., Toomanian, N., Heung, B., Behrens, T., Mosavi, A., Band, S., Amirian-Chakan, A., Fathabadi, A., Scholten, T., 2021. Improving the spatial prediction of soil salinity in arid regions using wavelet transformation and support vector regression models. Geoderma 383, 114793. https://doi.org/10.1016/j.geoderma.2020.114793.

UN, 2022. Transforming our world: the 2030 Agenda for Sustainable Development | Department of Economic and Social Affairs [WWW Document]. URL https://sdgs.un.org/2030agenda (accessed 12.20.22).

USGS, 2022. Landsat 8 | U.S. Geological Survey [WWW Document]. URL https://www.usgs.gov/landsat-missions/landsat-8 (accessed 11.21.22).

Wang, F., Yang, S., Yang, W., Yang, X., Jianli, D., 2019. Comparison of machine learning algorithms for soil salinity predictions in three dryland oases located in Xinjiang Uyghur Autonomous Region (XJUAR) of China. Eur. J. Remote Sens. 52, 256–276. https://doi.org/10.1080/22797254.2019.1596756.

Zarei, A., Hasanlou, M., Mahdianpari, M., 2021. A comparison of machine learning models for soil salinity estimation using multi-spectral earth observation data. ISPRS Ann. Photogramm. Remote Sens. Spatial Inf. Sci. V-3–2021, 257–263. doi: 10.5194/isprs-annals-V-3-2021-257-2021.

Zhou, Y., Chen, S., Hu, B., Ji, W., Li, S., Hong, Y., Xu, H., Wang, N., Xue, J., Zhang, X., Xiao, Y., Shi, Z., 2022. Global soil salinity prediction by open soil Vis-NIR spectral library. Remote Sens. (Basel) 14, 5627. https://doi.org/10.3390/rs14215627.